J|A|C|S
ARTICLES
Published on Web 03/01/2006

Potential Energy Landscape of the Photoinduced Multiple Proton-Transfer Process in the Green Fluorescent Protein: Classical Molecular Dynamics and Multiconfigurational Electronic Structure Calculations

Oriol Vendrell, Ricard Gelabert,* Miquel Moreno, and José M. Lluch

Contribution from the Departament de Química, Universitat Autònoma de Barcelona, 08193, Bellaterra, Barcelona, Spain

Received July 25, 2005; E-mail: ricard.gelabert@uab.es

Abstract: The green fluorescent protein proton wire operating upon photoexcitation of the internally caged chromophore is investigated by means of classical molecular dynamics and multiconfigurational electronic structure calculations. The structure of the proton wire is studied for the solvated protein, showing that the wire is likely to be found in a configuration ready to operate as soon as the chromophore is photoexcited, and leading to a total of three proton translocations in the vicinity of the chromophore. Multiconfigurational CASSCF and CASPT2 calculations provide a detailed overview of the energy landscape of the proton wire for the ground electronic state S_0, the photoactive $^1\pi\pi^*$ state, and the charge-transfer $^1\pi\sigma^*$ state. The results allow discussion of the operation of the wire in terms of the sequence of proton-transfer events and the participation of each electronic state.

Introduction

Green fluorescent protein (GFP) is an important fluorescent marker in cell biology, exhibiting a complex photophysics and photochemistry that has been the subject of many investigations during the last 10 years.[1] Experimental[2−14] as well as theoretical[15−24] works have been mainly devoted to shedding light into the complex photophysics of the protein, arising from the internally caged chromophore and the nearby residues. A great part of the interest on GFP comes from the multiple proton relay system that operates in it after photoexcitation. It is widely accepted that the proton wire operating inside the GFP proceeds through a multiple proton-transfer process connecting the chromophore with a glutamate residue in three proton hops. Such a pathway was originally proposed on the basis of X-ray measurements of the protein structure.[25] Recent experiments using ultrafast transient infrared spectroscopy[14] give further evidence in favor of this pathway. The proton wire operates inside the GFP upon photoexcitation of the chromophore (Cro) to the photoactive $^1\pi\pi^*$ state. The Cro residue is hydrogen-bonded to an internally caged water molecule (Wat25) in the same cavity. Wat25 is hydrogen-bonded to a serine residue (Ser205) that finally connects to a glutamate residue (Glu222) and completes the wire. Photoactivated proton wires have been receiving much attention in recent times[26] due to their technological applicability and biological importance; photoactivated proton transfer from a chromophore to a nearby solvent molecule has also received much attention.[27]

(1) Zimmer, M. *Chem. Rev.* **2002**, *102*, 759−781.
(2) Chattoraj, M.; King, B. A.; Bublitz, G. U.; Boxer, S. G. *Proc. Natl. Acad. Sci. U.S.A.* **1996**, *93*, 8362−8367.
(3) Lossau, H.; Kummer, A.; Heinecke, R.; Pöllinger-Dammer, F.; Kompa, C.; Bieser, G.; Jonsson, T.; Silva, C. M.; Yang, M. M.; Youvan, D. C.; Michel-Beyerle, M. E. *Chem. Phys.* **1996**, *213*, 1−16.
(4) Creemers, T. M. H.; Lock, A. J.; Subramaniam, V.; Jovin, T. M.; Volker, S. *Nat. Struct. Biol.* **1999**, *6*, 557−560.
(5) Striker, G.; Subramaniam, V.; Seidel, C. A. M.; Volkmer, A. *J. Phys. Chem. B* **1999**, *103*, 8612−8617.
(6) Mauring, K.; Suisalu, A.; Kikas, J. *J. Lumin.* **2000**, *87*−*89*, 812−814.
(7) Cotlet, M.; Hofkens, J.; Maus, M.; Gensch, T.; Van der Auweraer, M.; Michiels, J.; Dirix, G.; Van Guyse, M.; Van der Leyden, J.; Visser, A. J. W. G.; De Schryver, F. C. *J. Phys. Chem. B* **2001**, *105*, 4999−5006.
(8) Winkler, K.; Lindner, J. R.; Subramaniam, V.; Jovin, T. M.; Vohringer, P. *Phys. Chem. Chem. Phys.* **2002**, *4*, 1072−1081.
(9) Stubner, M.; Schellenberg, P. *J. Phys. Chem. A* **2003**, *107*, 1246−1252.
(10) Mandal, D.; Tahara, T.; Meech, S. R. *J. Phys. Chem. B* **2004**, *108*, 1102−1108.
(11) Vengris, M.; van Stokkum, I. H. M.; He, X.; Bell, A. F.; Tonge, P. J.; van Grondelle, R.; Larsen, D. S. *J. Phys. Chem. A* **2004**, *108*, 4587−4598.
(12) Agmon, N. *Biophys. J.* **2005**, *88*, 2452−2461.
(13) Jung, G.; Wiehler, J.; Zumbusch, A. *Biophys. J.* **2005**, *88*, 1932−1947.
(14) Stoner-Ma, D.; Jaye, A. A.; Matousek, P.; Towrie, M.; Meech, S. R.; Tonge, P. J. *J. Am. Chem. Soc.* **2005**, *127*, 2864−2865.
(15) Voityuk, A. A.; Michel-Beyerle, M. E.; Rosch, N. *Chem. Phys.* **1998**, *231*, 13−25.
(16) Weber, W.; Helms, V.; McCammon, J. A.; Langhoff, P. W. *Proc. Natl. Acad. Sci. U.S.A.* **1999**, *96*, 6177−6182.
(17) Reuter, N.; Lin, H.; Thiel, W. *J. Phys. Chem. B* **2002**, *106*, 6310−6321.
(18) Lill, M. A.; Helms, V. *Proc. Natl. Acad. Sci. U.S.A.* **2002**, *99*, 2778−2781.
(19) Marques, M. A. L.; Lopez, X.; Varsano, D.; Castro, A.; Rubio, A. *Phys. Rev. Lett.* **2003**, *90*, 258101.
(20) Toniolo, A.; Ben-Nun, M.; Martinez, T. J. *J. Phys. Chem. A* **2002**, *106*, 4679−4689.
(21) Toniolo, A.; Granucci, G.; Martinez, T. J. *J. Phys. Chem. A* **2003**, *107*, 3822−3830.
(22) Martin, M. E.; Negri, F.; Olivucci, M. *J. Am. Chem. Soc.* **2004**, *126*, 5452−5464.
(23) Zhang, R. B.; Nguyen, M. T.; Ceulemans, A. *Chem. Phys. Lett.* **2005**, *404*, 250−256.
(24) Vendrell, O.; Gelabert, R.; Moreno, M.; Lluch, J. M. *Chem. Phys. Lett.* **2004**, *396*, 202−207.
(25) Brejc, K.; Sixma, T. K.; Kitts, P. A.; Kain, S. R.; Tsien, R. Y.; Ormo, M.; Remington, S. J. *Proc. Natl. Acad. Sci. U.S.A.* **1997**, *94*, 2306−2311.
(26) Tanner, C.; Manca, C.; Leutwyler, S. *Science* **2003**, *302*, 1736−1739.
(27) Domcke, W.; Sobolewski, A. L. *Science* **2003**, *302*, 1693−1694.

10.1021/ja0549998 CCC: $33.50

Experimental studies on the photophysics and photochemistry of GFP are usually interested in the overall cycle occurring upon photon absorption. The number of experiments concerning the three-step proton wire operating inside the protein is enormous,[2−14] whereas there is comparatively less theoretical work on the simulation and modeling of the three proton-transfer processes that constitute the photoactivated proton wire. Some theoretical studies have focused on the nonradiative deactivation pathways of the photoexcited chromophore,[16,20−22] involving mainly bond torsions that lead to a loss of planarity. Other theoretical studies have been devoted to reproduce the electronic spectra of the GFP chromophore, using either semiempirical[15] or time-dependent density functional methods (TDDFT).[19]

Time-resolved spectroscopic measurements led to the proposal of a three-state (structures) model.[2] Basically (in this brief discussion we keep the same nomenclature as in the original article), the A structure, namely the neutral chromophore, can be electronically excited at 400 nm to A*. Then A* evolves in a picosecond time scale to I*, which can either decay to the ground-state I and then return to A or evolve to B*, which in turn relaxes to the long-lived structure B. The A form is believed to contain the chromophore in neutral form, whereas I and B are thought to correspond to the chromophore in anionic form. Variations of this basic model have been proposed in other experimental works.[4,5,7] Lill and Helms[18] gave a first simulation of the three-step proton wire using a nearly classical molecular dynamics method. They concluded that the multiple proton transfer is triggered by the transfer of the phenolic proton from Cro to Wat25. The two following proton-transfer events, namely Wat25 → Ser205 and Ser205 → Glu222, would then proceed in a few tens of femtoseconds through a barrierless process. However, the first proton-transfer step was forced in the simulations, so that they were started from the deprotonated chromophore form, excluding the possibility of a fully concerted mechanism or the initial transfer of any of the other two protons. Their calculations were based on proton-transfer barrier estimations for general donor−acceptor pairs[28] used to derive proton-hop probabilities at each time step.[29,30] It has recently been shown[24] that the protonation of the Wat25 molecule may be a more complex process than could be anticipated at first sight, maybe involving an (apparent) electronic state crossing between the photoactive $^1\pi\pi^*$ electronic state and a $^1\pi\sigma^*$ charge-transfer state from the chromophore to the nearby water molecule. This kind of process appears to be a general trend of many organic chromophores[31,32] as well as of DNA base pairs.[33] Its importance to the photophysics of GFP is an issue being considered in the present work.

To our knowledge, there are no studies yet on the photoexcited GFP proton wire based on high-level electronic structure calculations of a relevant model, where all the possible proton-transfer events are analyzed from ab initio electronic excited-state energy calculations. In this study, we analyze the proton wire using multiconfigurational electronic structure calculations, and we obtain the proton-transfer energy profiles connecting all the possible protonation states of the wire on the ground electronic state S_0, the photoactive first $^1\pi\pi^*$ electronic state, and the $^1\pi\sigma^*$ charge-transfer electronic state. To devise a meaningful model for the electronic calculations, a classical dynamics study of the complete solvated protein was previously performed with focus on the relative positions of the chromophore and proton wire residues and their geometries.

The aim of this work is to provide a clear view of the energetics of the proton wire operating inside GFP and the role of the different electronic states. These results will contribute to a better understanding of the photochemical properties of the protein in conjunction with information coming from well-devised experiments. The article is organized as follows. Section 2 provides the computational details of the molecular dynamics simulations and the multiconfigurational electronic structure calculations. Subsections 3.1 and 3.2 contain the main results and discussion on the molecular dynamics simulations and the electronic structure calculations, respectively. Finally, section 4 summarizes the results and gives the overall conclusions.

2. Computational Details

2.1. Molecular Dynamics Simulations. Molecular dynamics simulations were performed starting from the 1EMB Protein Data Bank entry.[25] The CHARMM program,[34] 28b2 version, was used through all the simulations, in conjunction with the CHARMM 22 force field.[35] The neutral form of the chromophore of the GFP protein was described by means of the parameter set derived by Thiel and co-workers.[17]

The simulated system consists of the protein solvated in a sphere of radius 37 Å formed by 5531 water molecules of TIP3 type[36] and a total of 20 236 atoms. The position of the hydrogens of the overall system was obtained using the HBUILD command[37] of CHARMM. A 1-fs time step was used in the molecular dynamics propagation. The system was simulated using Newtonian dynamics inside the inner 32 Å region starting from the center of mass of the system and Langevin dynamics on the outer 5 Å shell.[38] The temperature was fixed at 300 K during the entire production simulation. The list of atoms belonging to the buffer region was updated every five steps. The buffer region was described by a friction coefficient of 62 ps^{-1}, and a quartic potential with force constant equal to 0.2 kcal/mol·$Å^{-4}$ starting at 35.5 Å from the center of mass of the system was used to prevent water molecules from the outer shell to evaporate. At no time during the simulation did a protein residue enter the buffer region.

The equilibration protocol prior to the production dynamics was as follows. The overall system was first minimized for 200 steps where all the coordinates of the protein and oxygen atoms corresponding to the crystallization waters were kept frozen. Such minimization was intended to release the bad contacts generated during the solvation of the system. On a subsequent minimization of 200 steps, all the atoms were allowed to move, and the backbone atoms were subjected to a harmonic potential with a force constant of 10.0 kcal/mol·$Å^{-2}$ with respect to crystal structure positions. A third minimization was then performed with no restrictions for another 100 steps. The system was then heated in three steps. In all of them, the backbone atoms evolved under an extra harmonic potential with a force constant of 10.0 kcal/mol·$Å^{-2}$ with respect to the last minimization positions. First, 10 000 steps of dynamics were performed, starting at a temperature of 20 K that was raised to 100 K at a rate of 1 K/step, remaining then at 100

(28) Lill, M. A.; Helms, V. *J. Chem. Phys.* **2001**, *114*, 1125−1132.
(29) Lill, M. A.; Helms, V. *J. Chem. Phys.* **2001**, *115*, 7985−7992.
(30) Lill, M. A.; Helms, V. *J. Chem. Phys.* **2001**, *115*, 7993−8005.
(31) Sobolewski, A. L.; Domcke, W. *J. Phys. Chem. A* **2001**, *105*, 9275−9283.
(32) Sobolewski, A. L.; Domcke, W.; Dedonder-Lardeux, C.; Jouvet, C. *Phys. Chem. Chem. Phys.* **2002**, *4*, 1093−1100.
(33) Sobolewski, A. L.; Domcke, W. *Eur. Phys. J. D* **2002**, *20*, 369−374.
(34) Brooks, B. R.; Bruccoleri, R. E.; Olafson, B. D.; States, D. J.; Swaminathan, S.; Karplus, M. *J. Comput. Chem.* **1983**, *4*, 187−217.
(35) MacKerell, A. D., Jr.; et al. *J. Phys. Chem. B* **1998**, *102*, 3586−3616.
(36) Jorgensen, W. L.; Chandrasekhar, J.; Madura, J. D.; Impey, R. W.; Klein, M. L. *J. Chem. Phys.* **1983**, *79*, 926−935.
(37) Brunger, A. T.; Karplus, M. *Proteins: Struct., Funct., Genet.* **1988**, *4*, 148−156.
(38) Brooks, C. L.; Brunger, A.; Karplus, M. *Biopolymers* **1985**, *24*, 843−865.

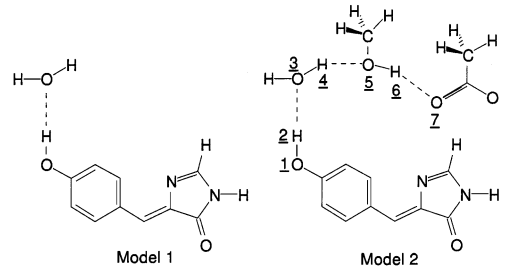

Figure 1. Schematic representation of the two models investigated in the quantum chemical calculations.

K until the dynamics was finalized. This procedure was then repeated from 100 to 200 K and finally from 200 to 300 K. Once the temperature was set at 300 K, the backbone constraints had to be smoothly released. To do so, the system was propagated for 10 000 steps with a force constant of 5.0 kcal/mol·Å^{-2}. Then, 10 000 steps were propagated with a force constant of 1.0 kcal/mol·Å^{-2}. Finally, 10 000 steps of totally unconstrained dynamics were run. The system was then considered ready for production simulations at 300 K.

2.2. Quantum Chemistry Calculations. The quantum chemistry calculations performed correspond to two models, which are depicted in Figure 1. In model 1, the chromophore and the closest water molecule are considered. The H_2O molecule is placed to mimic its position in the proton wire, and we note that it differs from a previous, related study.[24]

The more extended model, model 2, also includes the residues giving place to the proton wire inside the protein cavity. The Ser205 residue is modeled by a methanol molecule, while the Glu222 residue is modeled by an acetate molecule. Both models are set to have C_s symmetry, and the chromophore lies on the symmetry plane. This considerably reduces the computational effort, allowing us to perform calculations that would be otherwise even more computationally demanding. It also permits a more natural analysis and characterization of the two involved electronic excited states, since they belong to different symmetry representations of the C_s point group. The analysis of the classical trajectories of the whole solvated protein, to be discussed in section 3.1, reveals that the chromophore is close to planarity most of the time and that the proton wire is close to the plane defined by the chromophore. Deactivation pathways from the $^1\pi\pi^*$ state to the S_0 state will exist for the chromophore involving a loss of planarity,[16,20,21] which is not the subject of our investigation. The fact that fluorescence is observed during a few nanoseconds when the GFP is excited, a much longer time than the proton wire needs to operate, means that setting planarity based on the molecular mechanics simulations is not a severe assumption when studying the proton wire mechanism.

Complete active space self-consistent field (CASSCF) and complete active space with perturbation theory corrections (CASPT2)[39] calculations were performed on the two models using a 6-31++G(d,p) basis set with polarization and diffuse functions for the water molecule atoms, the oxygen atoms belonging to the wire and the three transferrable protons. For the rest of the atoms, a 6-31G basis set was used. Diffuse functions are important to describe the $^1\pi\sigma^*$ charge-transfer state since the water molecule is receiving a net electron coming from the chromophore.[24,31] An active space of six active orbitals with six electrons was used in all the multiconfigurational calculations on the ground electronic state S_0, the $^1\pi\pi^*$, and $^1\pi\sigma^*$ states. The $^1\pi\pi^*$ state energies were calculated within an active space consisting of the three highest occupied and the three lowest unoccupied π orbitals belonging to the chromophore molecule. For the $^1\pi\sigma^*$ state, the highest energy π^* orbital in the active space was substituted by the lowest unoccupied σ orbital. A similar active space has been already used in electronic structure calculations on the proton transfer from phenol to water and ammonia clusters[31] and in calculations considering the GFP chromophore and the Wat25 molecule.[24] In this work, we will refer to this active space as (6,6) for brevity. To check convergence with respect to the active space used, the energies of the S_0, $^1\pi\pi^*$, and $^1\pi\sigma^*$ electronic states of the eight structures corresponding to the eight possible protonation states of the proton wire were recalculated using the same atomic orbital basis set as above, but using an active space of nine orbitals with eight active electrons. In this set of electronic structure calculations, the active space was kept the same for the three electronic states. The active space consisted of the four highest occupied and the four lowest unoccupied orbitals of π symmetry and the lowest unoccupied σ orbital. This selection of active space will be referred to as (9,8) in this work. For each considered geometry, the three electronic states of interest were calculated separately (i.e., no state average calculations were performed). All the multiconfigurational calculations were performed within the MOLCAS 6 set of programs.[40]

3. Results and Discussion

3.1. Molecular Dynamics: Structure of the Proton Wire. Classical molecular dynamics simulations, which were intended to inspect the structural features of the chromophore and the proton wire in its surroundings, were performed on the solvated GFP protein. The main focus was on the geometry of the chromophore along the molecular dynamics simulations, as well as the spatial disposition of the proton wire with respect to it. Figure 2a shows the chromophore and the proton wire, which is taken from one of the molecular dynamics configurations. In this configuration, the three oxygen−oxygen distances involved in the proton wire are 2.85, 2.94, and 2.55 Å, respectively. Note that, for this particular configuration, the first two hydrogen bonds appear at distances slightly longer as compared to the mean distance over all the averaged population (Figure 3). As indicated from X-ray mesurements, the wire is formed by a crystallographic water molecule close to the phenolic moiety of the Cro residue, Wat25, the Ser205 residue, and the Glu222 residue.[25] Cro and the other three groups are connected by hydrogen bonds. Once Cro is photoexcited, the proton wire connecting Cro with Glu222 is able to operate due to differences in the overall potential energy function shape between the S_0 and the excited states.

The solvated GFP system was propagated for half a nanosecond under the conditions described before, and a configuration was saved every 5 ps, thus amounting to 100 configurations. Those constitute the basis of the structural analysis of the system. In Figure 3, the frequencies of appearance for the distances between the two oxygen atoms forming each of the three hydrogen bonds involved in the proton wire are plotted over the population of 100 configurations. The distances correspond to the pairs of atoms 1−3, 3−5, and 5−7, labeled in Figure 1.

The same information, now for the O−H−O angles of the three hydrogen bonds, is plotted in Figure 4. The atoms involved in the monitored angles are 1−2−3, 3−4−5, and 5−6−7. From the molecular dynamics simulations, the proton wire is well-formed most of the time. Oxygen−oxygen distances are centered at around 2.7−2.8 Å, except the third hydrogen bond, which is slightly shorter. This is because Glu222 is initially a negatively charged species, thus forming a shorter-than-average hydrogen bond. As for the O−H−O angles of the hydrogen

(39) Andersson, K.; Malmqvist, P.-Å.; Roos, B. O. *J. Chem. Phys.* **1992**, *96*, 1218−1226.

(40) Andersson, K.; et al. *MOLCAS 6.0: User's Guide*; Lund University: Lund, Sweden, 2004.

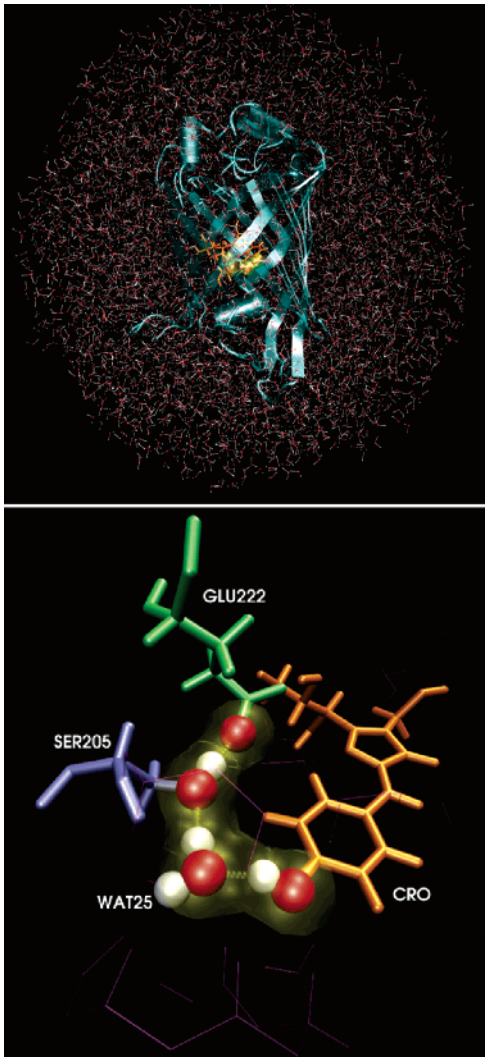

Figure 2. Solvated GFP (top) and detail of the inner chromophore and proton wire (bottom). The donor and acceptor atoms, transferable protons, and the Wat25 water molecule are represented in red and white. The region corresponding to the proton wire is highlighted for clarity purposes.

bonds, most of the time they are between 160 and 170°. Thus, one can conclude that most of the time the proton wire is likely to be found in a configuration adequate for the multiple proton transfer to occur. This is well in agreement with more general molecular dynamics simulations devoted to study the hydrogen bond network around the chomophore in the protein environment.[41]

Another structural feature that is of interest is the planarity of the chromophore inside the protein cavity. It has been addressed in the past by Zimmer and co-workers,[42] who monitored the two dihedral angles τ and ψ that correspond to the torsions along the two bonds connecting both rings of the chromophore. In this work, as a simple measure of the planarity of the overall residue, we have focused on the dihedral angle between the two rings of the chromophore. The information is depicted in Figure 5. The two rings spend most of the time near a planar conformation, but the distribution is not centered at 0°. The most probable angles are close to −8 and 8°,

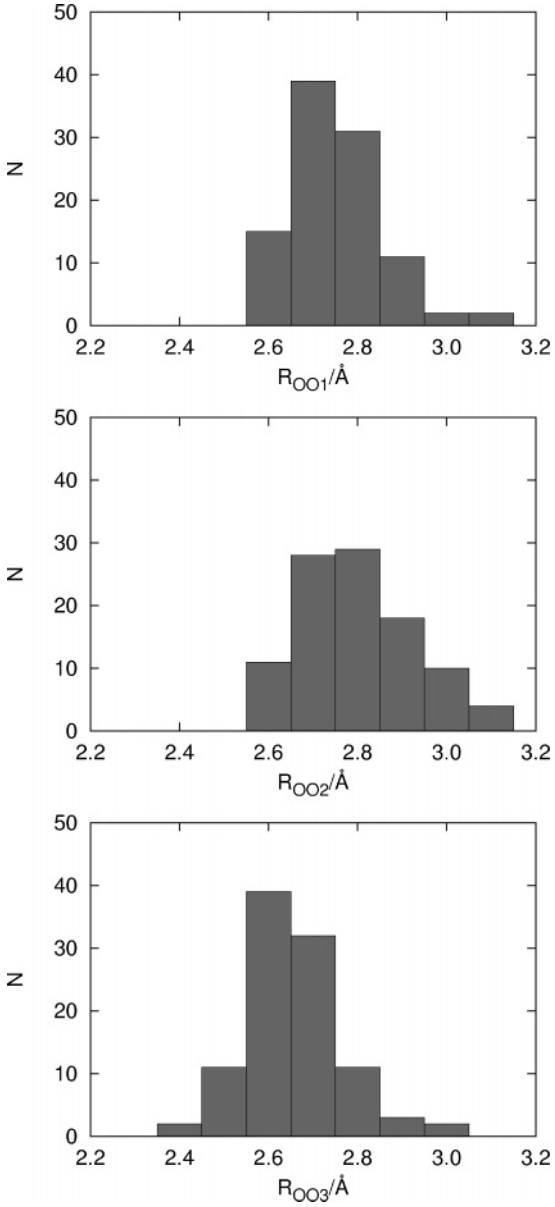

Figure 3. Histogram of the oxygen−oxygen distances implied in the proton wire. Cro−Wat25 (top), Wat25−Ser205 (middle), and Ser205−Glu222 (bottom). The values were sampled from classical molecular dynamics simulations.

indicating that the chromophore is most of the time only slightly out-of-plane.

3.2. Quantum Chemistry Calculations: Photochemistry of the Proton Wire. The analysis of the already introduced models 1 and 2 (Figure 1) is undertaken in this section. The results of model 1, which are complementary to a previous study,[24] serve as a reference point to understand the role of the wire residues in the overall multiple proton-transfer process.

The aim of the quantum chemistry calculations for model 2 (the model in which the complete proton wire is contained) is 2-fold. First, these calculations are intended to provide a picture of the potential energy landscape over which the proton wire operates, based on a static picture of the process in which discussion is centered around the idea of "protonation states" and will involve estimated exoergodicities and endoergodicities incurred when the proton wire evolves between any two of these protonation states. One could even try to study the dependence

(41) Nifosi, R.; Tozzini, V. *Proteins: Struct., Funct., Genet.* **2003**, *51*, 378−389.
(42) Chen, M. C.; Lambert, C. R.; Urgitis, J. D.; Zimmer, M. *Chem. Phys.* **2001**, *270*, 157−164.

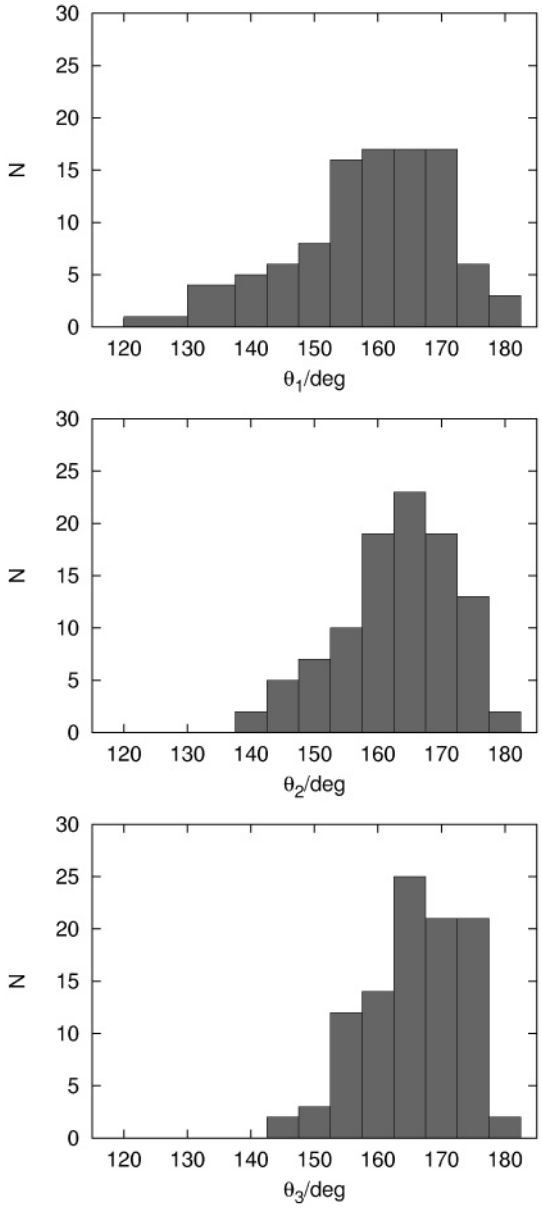

Figure 4. Histogram of the oxygen−proton−oxygen angles implied in the proton wire. Cro−Wat25 (top), Wat25−Ser205 (middle), and Ser205−Glu222 (bottom). The values were sampled from classical molecular dynamics simulations.

of these energetic magnitudes when each of the heavy atoms supporting the proton wire is allowed to relax and stabilize the system and in this way center the discussion in the values of potential energy barriers and relative stabilities when all the atoms in the wire are allowed to relax. In other words, one seemingly could carry out a study based on elements such as minimum energy paths (MEPs) connecting "minimum energy structures" and use them as a criterion to establish the operation of the wire, the sequence of motions, and rates of motion. At this point, it is worth highlighting that the proton transfer operating within GFP has been described as a very fast process.[2,3] Additionally, it is a very complex triple proton-transfer process, and thus quantum effects such as tunneling are expected to be very important in the operation of the proton wire. In a situation such as this, it is dubious whether a discussion based *solely* on reaction paths is meaningful, and actually several issues seem to point in the opposite direction:

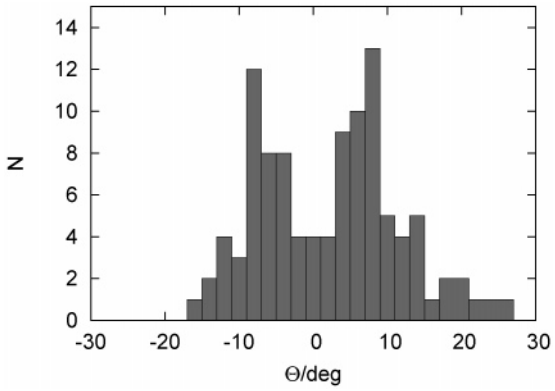

Figure 5. Histogram of the chromophore ring−ring dihedral angle. The values were sampled from classical molecular dynamics simulations.

the proton-transfer coordinate(s) will show strong curvatures and quantum effects such as corner-cutting tunneling are guaranteed to be present. This, together with the likely lack of ergodicity (in view of the speed of the process) will certainly question the validity of a discussion based on the localization of minimum energy structures where all atoms are allowed to relax, and determination of the proton-transfer barriers, among other reasons, because after the vertical Franck−Condon electronic transition the system does not start from the minimum in the excited electronic state.

For these reasons, the second aim of the calculations on model 2 is to provide a reasonable picture of the relevant potential energy surface (PES) describing the proton transfer in the wire, in addition to the minima and transition-state structures, to build up an as-accurate-as-possible multidimensional PES over which full quantum nuclear dynamics simulations can be performed (that is, involving explicit motion of all protons *and* heavy atoms that make up the wire). We believe that this is a more reliable and acceptable way of describing the ultrafast dynamics of the proton transfer in the wire. This quantum dynamics study over the PES that we present in this article and that is contained explicitly in the Supporting Information of this work is currently work in progress in our laboratory.

As mentioned before, calculations over model 2 are based on potential energy profile calculations for the three transferable protons. This analysis plays with the idea of protonation states, a protonation state being a structure in which each proton is within bonding distance (∼1 Å) to either its donor or acceptor atom. To refer to the different protonation states of the proton wire, a code of three characters is used, each one identifying the position of one of the protons. These are depicted and explained in Figure 6. The first character refers to the proton shared between Cro and Wat25, which can be either "C" or "W". The second character refers to the proton shared between Wat25 and Ser205, which can be either "W" or "S". In the same way, the last character can be either "S" or "G". States labeled with codes in which a character appears twice have two protons bonded to that residue. They have, hence, a formal positive charge located over the residue appearing twice in the code. Residues whose initials do not appear in a protonation state code have a formal negative charge in that protonation state. Both charged and noncharged groups of protonation states appear in red and in blue in Figure 6, respectively. Since there are three transferable protons, there are a total of $2^3 = 8$ protonation states. The idea of protonation states we are using does not assume

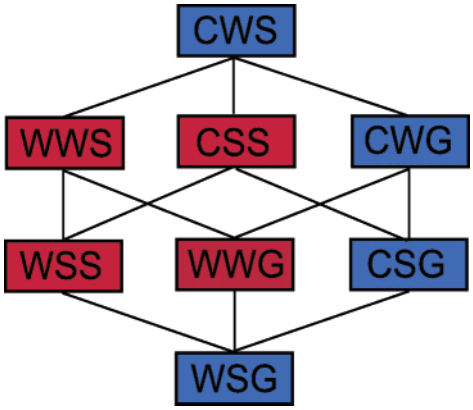

Figure 6. Schematic representation of the possible protonation states of the proton wire. Each code of three characters represents one of the eight possible limiting protonation states of the wire. Each character represents the position of one of the three protons, starting by the proton initially bound to the chromophore, the proton shared between the water molecule and the serine residue, and the proton shared between the serine residue and the glutamate residue, respectively. The first character may have the values "C" or "W", depending on whether the proton is in bonding distance to the chromophore or to the water molecule. Analogously, the second character may be "W" or "S", and the third one "S" or "G". Protonation states in blue have a formal negative charge in one of the positions along the chain. Protonation states in red have one formal positive charge and two formal negative charges along the chain. Straight lines identify paths involving the transfer of a single proton. All paths implying the transfer of a single proton at a time are depicted in the figure.

anything about their stability; it is simply a convenient way of referring to the different structures and paths relevant to the proton wire. Using such convention, reactants are represented by (CWS), products are represented by (WSG), the situation in which only the proton shared by Cro and Wat25 has transferred would be given by WWS, and so on.

The minimization of the potential energy for model 2 at the CASSCF level of theory and the (6,6) active space in S_0 yields a structure where the O−O distances are 2.65 Å (Cro−Wat25), 2.59 Å (Wat25−Ser205), and 2.48 Å (Ser205−Glu222).

The 12 paths involving only the motion of any one proton along each path are represented in Figure 6. Each path has been explored at three donor−acceptor distances, thus leading to 36 energy profiles. For each hydrogen bond involving the transferring proton, three O−O distances corresponding to its donor and acceptor atoms have been studied, with values between 2.30 and 2.65 Å, intended to cover the domain of equilibrium distances in the S_0 electronic state and the shortest expected donor−acceptor distances in normal proton-transfer events (for precise values, see Supporting Information). The other two O−O distances (i.e., those for the hydrogen bonds that do not experience transfer) are kept frozen at their values for the minimum in S_0. Each energy profile consists of the evaluation of the potential energy at seven intermediate positions of the transferable proton between the corresponding donor and acceptor oxygen atoms. This scheme leads then to a total amount of 252 distinct geometries being considered. For each geometry, the S_0, $^1\pi\pi^*$, and $^1\pi\sigma^*$ electronic states are considered at both CASSCF and CASPT2 levels with the (6,6) active space, thus having performed a total of 1512 multiconfigurational potential energy evaluations. Technical details of the calculations can be found in section 2.2. The different structures have been generated with the protons lying on the straight line that connects donor and acceptor atoms, which is reasonable in view of the results of the molecular dynamics simulations presented above, especially Figure 4. The geometry of the rest of the system is kept frozen at the S_0 minimum energy geometry. We explore all the possible single proton-transfer paths connecting the reactants' (CWS) and the products' (WSG) structures as a way to gather information on the nature of the proton wire mechanism, its energetics, and the role of the different electronic states. Full information on all the performed calculations is available as Supporting Information and will be used to construct a potential energy surface to dynamically simulate the multiple proton-transfer process.

A main point of interest in the present discussion is the analysis of the proton-transfer energy profiles corresponding to the proton moving from Cro to Wat25. The coordinate used to represent the proton position corresponds to the signed distance of the proton to the point halfway between both donor and acceptor atoms. The potential energy profiles of the $^1\pi\pi^*$ and $^1\pi\sigma^*$ electronic states at both CASSCF and CASPT2 levels with the (6,6) active space are found in Figure 7. The O−O distance for the proton transfer from Cro to Wat25 is held fixed at 2.65 Å in all cases. The geometry of the other two hydrogen bonds is kept frozen at the geometries of the minimum in S_0 while the first proton is being transferred: the O−O distance in the Wat25 to Ser205 transfer is 2.59 Å, and that of the Ser205 to Glu222 is 2.48 Å, while the corresponding protons are bound to the donor oxygen atoms (i.e., within 1 Å of it). Figure 7a,b represents the proton-transfer energy profiles from Cro to Wat25 for model 1 (Figure 1) at the CASSCF and CASPT2 levels, respectively, and the (6,6) active space. The $^1\pi\pi^*$ electronic state is strongly destabilized due to the charge separation induced as the proton moves from the chromophore to the water molecule. The $^1\pi\sigma^*$ electronic state intersects the photoactive $^1\pi\pi^*$ state at both CASSCF and CASPT2 levels of theory. The main difference between the CASSCF and CASPT2 results is an extra stabilization of the $^1\pi\pi^*$ state at the CASPT2 level, resulting in a later crossing of both states. The same results were also found in one of our previous studies,[24] where the water molecule hydrogen atoms were set out-of-plane, contrary to the current model 1, where they are set in-plane, more in accordance to the results coming from the molecular dynamics simulations. Profiles corresponding to model 2 are found in Figure 7c−f. In Figure 7c,d, the results corresponding to the proton transfer to Wat25 are represented. In terms of the already introduced protonation states, the analyzed profiles correspond to the (CWS) → (WWS) process. The presence of the rest of the wire stabilizes the $^1\pi\pi^*$ electronic state when the proton is transferred. The $^1\pi\sigma^*$ electronic state appears to be less sensitive to the presence of the rest of the chain. Hence, the crossing appears at longer values of the proton-transfer coordinate, as compared to that in model 1. As seen before, at the CASPT2 level the $^1\pi\pi^*$ presents an extra stabilization with respect to the CASSCF results, leading to a nearly noncrossing situation (Figure 7d). Figure 7e,f corresponds to the (CSS) → (WSS) process, the proton transfer from Cro to Wat25 once Wat25 has already transferred one proton to Ser205. It is interesting to note how the $^1\pi\sigma^*$ state is clearly destabilized when the proton initially at Wat25 is at the reactants side, Ser205. This is because the $^1\pi\sigma^*$ state is an electron-transfer state, implying an electron transfer from Cro to Wat25.[24] When the proton from Cro is not yet transferred, the $^1\pi\sigma^*$ state corresponds formally to an extra electron on a

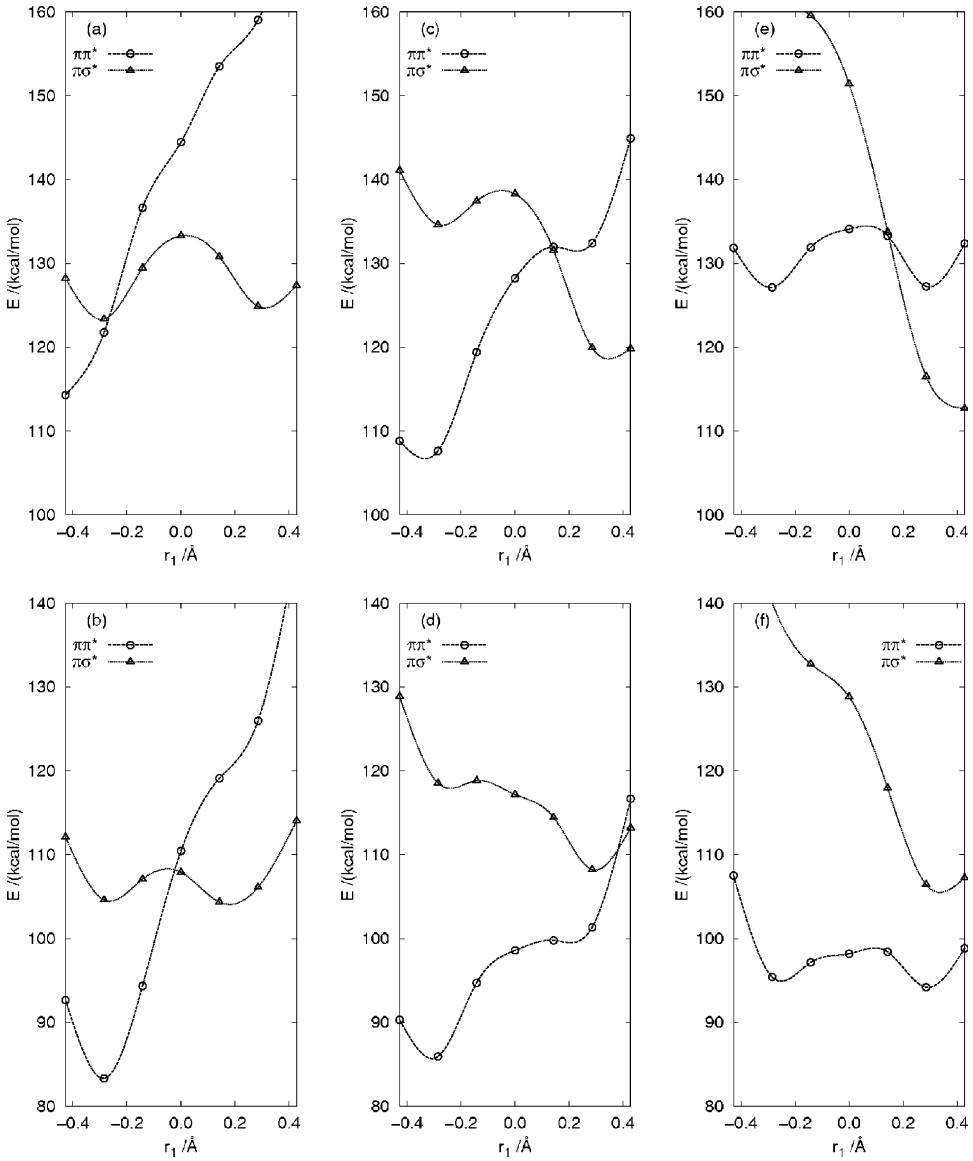

Figure 7. Proton-transfer potential energy profiles corresponding to the translocation of the first proton from the chromophore to the nearby water molecule at CASSCF (top) and CASPT2 (bottom) levels of theory with the (6,6) active space. The energy profiles correspond to both the photoactive $^1\pi\pi^*$ and $^1\pi\sigma^*$ electronic states. (a,b) Transfer to an isolated water molecule. (c−f) Transfer when the rest of the chain is present. (c,d) Situation in which the chromophore transfers the phenolic proton to a water molecule, (CWS) → (WWS); (e,f) Chromophore transferring its proton once the water has already protonated the serine residue, (CSS) → (WSS). The energy origin is set on the ground state of the most stable structure for both models 1 (a,b) and 2 (c−f). The abscissa value r_1 is the signed distance of the proton to the point halfway between the donor and acceptor atoms.

OH^- fragment. As expected from previous results, at the CASPT2 level an extra stabilization of the $^1\pi\pi^*$ state with respect to the $^1\pi\sigma^*$ state causes the intersection between both electronic states to disappear (Figure 7f).

One should bear in mind that Wat25 is involved in additional hydrogen bonds in the protein cavity, which would stabilize the situation corresponding to a protonated water molecule. Additionally, Glu222 is involved in an extra hydrogen bond with the chromophore, which would partially destabilize it as a proton acceptor species. As an example, a recent computational work by Zhang et al. discusses the importance of the residue His148, which is able to form a hydrogen bond with either the phenolic oxygen of the chromophore or the water molecule.[23] Thus, it is obvious that the real system is more complex than the model we have used here. The inclusion of more residues in high-level electronic calculations to build more accurate models is an issue to be considered as the computational power allows.

In Table 1, the potential energy of the different protonation states for each relevant electronic state can be found. The multiconfigurational calculations leading to the results in Table 1 have been performed using two different active spaces (see section 2.2 for details). The (6,6) active space is the one also used for the computation of all the energy profiles corresponding to the different 252 geometries considered. An active space of nine orbitals and eight electrons (henceforth, (9,8)) is used to recompute the eight structures appearing in Table 1, so as to give more accurate results and to validate the smaller active space. At the CASPT2 level, most of the results obtained for the (9,8) active space are mostly within 3 kcal/mol of the results obtained for the (6,6) active space, and the changes of the relative energies between the different configurations considered

Table 1. Energies (in kcal/mol) of the Different Protonation States of the Wire, at the S_0, $^1\pi\pi^*$, and $^1\pi\sigma^*$ Electronic States[a]

protonation state	S_0	$^1\pi\pi^*$	$^1\pi\sigma^*$
		CASSCF	
CWS	0.0 (0.0)	110.7 (105.9)	131.1 (134.9)
WWS	45.1 (44.9)	139.7 (136.0)	111.0 (119.1)
CSS	27.6 (27.9)	134.4 (130.0)	163.3 (167.1)
CWG	12.8 (12.7)	121.6 (117.0)	152.8 (156.4)
WSS	41.0 (35.5)	131.0 (131.7)	107.7 (116.1)
WWG	46.7 (41.2)	139.1 (138.6)	121.6 (130.1)
CSG	17.0 (13.4)	120.4 (116.5)	160.1 (163.0)
WSG	22.8 (16.8)	110.7 (111.6)	98.9 (107.4)
		CASPT2	
CWS	0.0 (0.0)	82.2 (85.5)	119.5 (119.8)
WWS	40.9 (40.8)	105.4 (104.8)	105.9 (108.4)
CSS	21.5 (21.3)	99.6 (102.8)	144.1 (144.5)
CWG	12.5 (12.5)	92.6 (95.6)	140.0 (140.3)
WSS	34.8 (31.3)	93.8 (96.4)	104.6 (106.6)
WWG	43.1 (45.3)	104.6 (108.5)	119.6 (121.5)
CSG	15.5 (14.4)	86.8 (86.1)	142.0 (142.0)
WSG	18.4 (20.8)	75.2 (77.6)	98.8 (101.2)

[a] The given energies correspond to the (9,8) active space. Values in parentheses correspond to the (6,6) active space.

are not significant for the discussion in this article. The eight structures out of 252 collected in Table 1 have been selected with the following criteria: the geometry of the proton wire, as to the distances between all the donor and acceptor atoms, is held fixed at the geometry of the minimum in S_0. Each protonation state structure corresponds to a structure with the three transferable protons at 1.0 Å either from the donor oxygen atom or from the acceptor oxygen atom. These protonation states do not necessarily represent stable structures, and in some cases the path from a protonation state to another implies a steady increase in potential energy. However, the protonation states constitute a set of points adequate to map the overall surface and unravel its main characteristics. It is interesting to see how the translocation of the three involved protons is highly endoergic on the S_0 surface, while it is exoergic on the $^1\pi\pi^*$ and $^1\pi\sigma^*$ surfaces at the CASPT2 level of calculation and only slightly endoergic at the CASSCF level of theory for the $^1\pi\pi^*$ case. At the CASSCF level, the $^1\pi\pi^*$ and $^1\pi\sigma^*$ states cross each other when the proton initially at Cro is transferred, independent of the position of the other two transferable protons. One can compare the energy of the (CXY) and the corresponding (WXY) protonation states to appreciate the dissociative nature of the $^1\pi\sigma^*$ electronic state toward the transfer of the first proton.

The number of different ways to go from (CWS) to (WSG) which involve single proton translocations is $3! = 6$, as can be seen by visually inspecting Figure 6. The analysis in terms of the protonation state energies provides interesting information about the mechanism of the photoexcited proton wire. The six paths (not to be confused with energy profiles: these paths map ways to go between fixed structures corresponding to protonation states) connecting (CWS) and (WSG) are given in Figure 8 at the CASPT2 level of theory, using the large (9,8) active space. Going from (CWS) to (WSG) is an endoergic process in S_0 that costs around 18 kcal/mol. Conversely, such a process is exoergic by 7.0 kcal/mol in the photoactive $^1\pi\pi^*$ electronic state and by around 20 kcal/mol in the charge-transfer $^1\pi\sigma^*$ electronic state. In all cases, the (CXY) → (WXY) (Cro to Wat25) proton transfers in the $^1\pi\sigma^*$ state are exoergic processes, clearly showing that it is a very dissociative electronic state toward chromophore deprotonation. However, the photoactive $^1\pi\pi^*$ state and the $^1\pi\sigma^*$ state never cross in the relevant regions at the CASPT2 level of theory, despite approaching each other when the proton initially at Cro is transferred to Wat25. They are closest in energy in the (WWS) configuration. It is worth noticing that the energy difference between (CXY) and (WXY) configurations decreases when going from the S_0 to the $^1\pi\pi^*$ electronic state, by 14−19 kcal/mol, making the $^1\pi\pi^*$ protonation of Wat25 from Cro an exoergic process in some proton wire configurations, as can be seen in Figure 8d−f. This is never the case in S_0, where deprotonating the chromophore is always an endoergic process. Inspecting the different paths in the $^1\pi\pi^*$ state, one realizes that, after first transferring any of the three protons, (CWS) → (WWS), (CWS) → (CSS), or (CWS) → (CWG), a downhill way to (WSG) always exists, except for the path in Figure 8c, whose higher protonation state appears after the second proton transfer. These paths correspond to Figure 8a,d−f. Of these paths, the most energetically favorable upon photoexcitation is the one in Figure 8d, which corresponds to first transferring the proton from Ser205 to Glu222, then from Wat25 to Ser205, and finally from the chromophore to Wat25. It is noteworthy that the aforementioned path is the only one that goes through all the protonation states in blue in Figure 6. The first proton transfer in this path costs between 10 and 12 kcal/mol, in both S_0 and $^1\pi\pi^*$ states. All the paths passing through structures with a formal positive charge and two formal negative charges along the chain (which in the naming convention used to identify the protonation states in this work are those states in which one character is repeated in the code, and they are depicted in red in Figure 6) involve higher energies. The fact that all the paths from (CWS) to (WSG) in $^1\pi\pi^*$ involve going first through a higher-in-energy protonation state is in accord with much of the experimental results indicating a mean proton-transfer time of around 12 ps.[2,3,14] The path in Figure 8a, starting with the (CWS) → (WWS) transfer, corresponds to the one proposed by Lill and Helms.[18] Despite being a downhill path after the proton initially at Cro transfers, the initial step is endoergic by roughly 23 kcal/mol.

Up to this point we have seen that the path in Figure 8d appears to be the most favorable nonconcerted (stepwise) path. The question remains open as to what happens for a hypothetical concerted mechanism. To complete the above discussion, then, the energy corresponding to a structure where the three transferable protons are centered between the corresponding oxygen atoms was evaluated at the CASPT2 level of theory with the (6,6) active space in the $^1\pi\pi^*$ electronic state, while the rest of the system was kept at the geometry of the minimum in S_0. Such a structure is not necessarily a real transition state, but its energy provides insight into the feasibility of a concerted mechanism to operate on the wire. On the S_0 electronic state, such a structure is located 30.7 kcal/mol above the (CWS) configuration. In ref 23, where only the S_0 state is considered, the concerted transition-state energy of the closest model to ours is reported to be 24.08 kcal/mol, in reasonable agreement with the value we found, considering the differences between both computational works. As for the $^1\pi\pi^*$ electronic state, this *concerted transfer* structure lies only 14.8 kcal/mol above the energy of the (CWS) configuration. This value should be compared to the energy difference between the (CWG) and (CWS) structures in $^1\pi\pi^*$ for the most favorable stepwise path

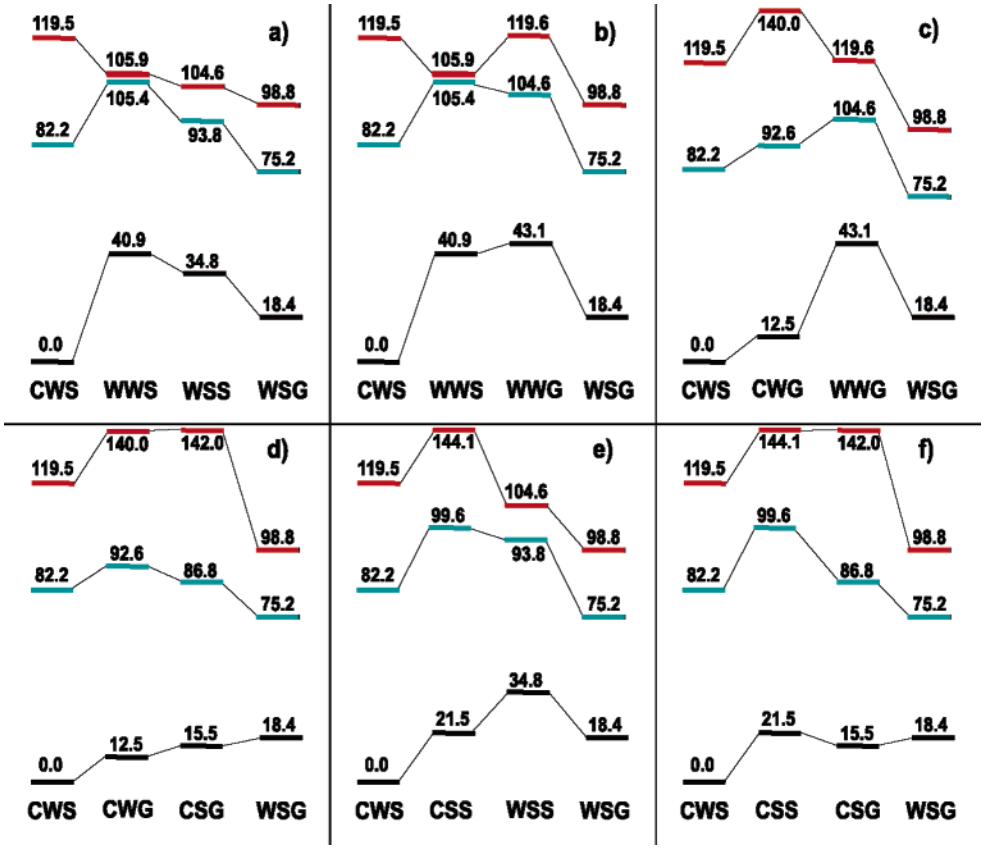

Figure 8. Relative stability of the protonation states connecting (CWS) and (WSG). Paths involving single proton hops are given. Energies correspond to the CASPT2 calculations using the larger (9,8) active space. S_0 state is given in black, $^1\pi\pi^*$ state appears in blue, and $^1\pi\sigma^*$ is depicted in red. Energies are given in kcal/mol. The protonation states involved in each path appear at the bottom of each profile representation.

found (Figure 8d) at the same level of calculation, this being 95.6 − 85.5 = 10.1 kcal/mol (see values in parentheses in Table 1). Such a small difference between both paths certainly does not exclude the possibility of a concerted mechanism to operate on the excited state upon photoexcitation, possibly competitively with a stepwise mechanism. We want to emphasize that it is not the aim of the present work to discern between a concerted or a stepwise mechanism, this issue being better addressed from a dynamical perspective. Certainly this is an interesting point to be considered soon.

The results presented up to now correspond to the system with the heavy atoms in the proton wire held fixed in the same positions as in the minimum in S_0. This could be a reasonable approximation taking into account that the process seems to be very fast after the vertical Franck−Condon electronic excitation. Allowing the different O−O distances to relax would lead to lower energies for the protonation states. However, because of the reasons stated at the beginning of section 3.2, the energetics that one could obtain in this way would be inadequate to draw definitive conclusions on the operativity of the proton wire, being necessary for this purpose a quantum dynamical study in which also the heavy atoms are allowed to move. In view of this, the results presented thus far give a reasonable picture of the energy landscape that underlies the proton wire, for both the stepwise and concerted possibilities, concluding that competition between both seems possible. As mentioned earlier, the complete PES obtained in this way is to be used for a complete quantum dynamical simulation involving also the heavy atoms in the wire.

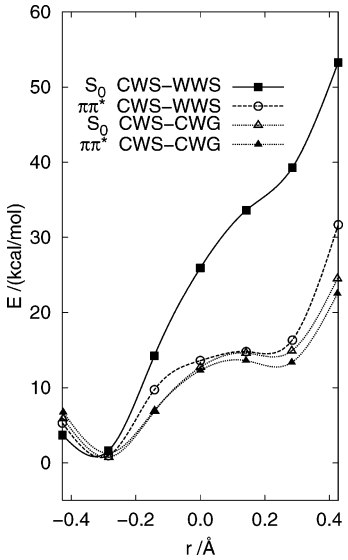

Figure 9. Proton-transfer energy profiles corresponding to the transfer from the chromophore to Wat25 and from Ser202 to Glu222, computed using the CASPT2 method with the small (6,6) active space. The energy profiles of the $^1\pi\pi^*$ electronic state have been shifted by −85 kcal/mol so that they can be visually compared to the S_0 profiles. *r* identifies the position of the transferring proton, in terms of the signed distance to the point halfway between the donor and acceptor atoms for the affected hydrogen bond.

Figure 9 depicts the potential energy profiles for the initial step in both the paths appearing in Figure 8a,d for the S_0 and $^1\pi\pi^*$ electronic states. In the first case, this corresponds to the transfer of the proton from Cro to Wat25, whereas in the second

case it represents the transfer of the proton from Ser205 to Glu222. The potential energy curves corresponding to the $^1\pi\pi^*$ state have been shifted by −85.0 kcal/mol to allow for visual comparison of the energy profiles discussed here. It has been already seen that the path in Figure 8d is the one that appears to be the most energetically accessible. However, the potential energy curves for the transfer of the proton from Ser205 to Glu222 are nearly identical in both the S_0 and $^1\pi\pi^*$ states (curves with full and empty triangles in Figure 9). Conversely, the potential energy profile corresponding to the deprotonation of the chromophore, as could be expected, is dramatically changed upon photoexcitation. In other words, photoexcitation causes local changes in the shape of the potential energy surface that clearly favor the Cro to Wat25 proton transfer. How does this fact affect the paths in Figure 8, parts a and d? The Cro to Wat25 proton transfer is the first step in the path in Figure 8a, leading to a high-energy WWS protonation state in S_0. This path is still energetically expensive in the $^1\pi\pi^*$ electronic state despite the stabilization due to the electronic excitation. On the contrary, that proton transfer is the last step of the path in Figure 8d. The energetic cost of the first step of this second path is low already in the S_0 state, and the photoexcitation reduces noticeably the energetic requirements of the second and third steps in the $^1\pi\pi^*$ electronic state. This is the reason the most favorable nonconcerted path is the one that initiates the chain of proton transfers at the other end of the chromophore, in this way pulling the proton motion along the wire.

Finally, the information reported thus far also allows for the discussion of the return path from the (WSG) to (CWS) protonation states, after decay into the S_0 electronic state from the $^1\pi\pi^*$ electronic state. Taking into account the starting and ending points of the proton transfers, the path in Figure 8d also represents the most favorable returning path, implying only an energy decrease. Of course, energy barriers could exist between the protonation states. It has been proved[2,3] that the (CWS) protonation state (form A in much of the related bibliography) is regenerated from the unrelaxed (WSG) protonation state (form I in related bibliography) in a fast process. Recently, the time scale for the ground-state recovery of form A from the intermediate I in the ground state has been estimated to be within 400 ps.[43] These facts agree with our data reporting the existence of a favorable return path on the S_0 potential energy surface. Therefore, it is likely that energy barriers along this path exist, otherwise a purely downhill process would not take 400 ps.

4. Conclusions

In this article, an exhaustive theoretical study of the proton wire operating in the green fluorescent protein (GFP) upon electronic excitation of the internally caged chromophore has been given. The results can be divided in two parts. First, we performed molecular mechanics simulations of the solvated GFP protein, starting from a well equilibrated structure. One hundred configurations were sampled over 0.5 ns of classical dynamics. The analysis of these configurations revealed that the proton wire is likely to be found in a favorable geometry to operate when the chromophore is photoexcited. A favorable geometry means that the three hydrogen bonds that constitute the wire remain at donor−acceptor distances of 2.6−2.8 Å, with the transferable protons well-aligned between donor and acceptor atoms. Also, the chromophore is, for most of the time, in a nearly planar conformation, with a twisting angle of less than 10° between both chromophore rings. The classical dynamics results also showed that the wire is close to the chromophore plane. On the basis of the classical dynamics simulations, we devised two models for the high-level electronic calculations, which were set to belong to the C_s point group. Model 1 consists only on the chromophore and the nearby water molecule, Wat25, whereas model 2 contains the rest of the wire where Ser205 is modeled by a methanol molecule and Glu222 is modeled by an acetate molecule.

Quantum chemistry calculations were performed on both models 1 and 2 for the S_0, $^1\pi\pi^*$, and $^1\pi\sigma^*$ electronic states using the multiconfigurational CASSCF and CASPT2 methods. For model 2, which considers the complete proton wire, 252 geometries were considered, scanning each possible single proton transfer at three donor−acceptor distances. Calculations done on model 2 are aimed at building up a realistic representation of the potential energy surface describing the operation of the proton wire, including motion of heavy atoms, on which to carry out quantum dynamical simulations at a later stage. Current results serve the purpose of revealing the nature of the potential energy landscape and qualitatively describe the likely evolution of the system, after vertical Franck−Condon photoexcitation, and without considering neither kinetic energy nor nuclear quantum effects. This study of model 2 allowed us to unravel some interesting properties of the wire energetics. The main difference between models 1 and 2 is that the curve crossing between the $^1\pi\pi^*$ and $^1\pi\sigma^*$ states vanishes when all the wire is considered, mainly due to the stabilization of the $^1\pi\pi^*$ state with respect to the $^1\pi\sigma^*$. This means that the $^1\pi\sigma^*$ electronic state is likely to be unimportant in the photochemistry of GFP. However, this curve crossing may play a role in gas-phase clusters involving the GFP chromophore and one or few water molecules.

The energies of the eight structures corresponding to possible limiting protonation states were then analyzed, focusing mainly on the photoactive $^1\pi\pi^*$ electronic state. The most energetically favorable way for the proton wire to operate is to transfer first a proton from the serine residue to the glutamate, then a proton from water to serine, and finally a proton from the chromophore to the water molecule. This is also the mechanism that implies the smaller charge separation along the chain. Such a mechanism, which starts by the transfer of the most distant proton from the chromophore, is somewhat counterintuitive, because the most noticeable changes in the potential energy surface upon photoexcitation normally occur in coordinates directly related to the chromophore itself. To clarify this point, we analyzed the proton-transfer energy profiles of both the proton transferring from the chromophore to the water molecule and the proton transferring from the serine to the glutamate residue. The energy profile corresponding to the transfer of a proton from the serine to the glutamate residue remains unaltered by the photoexcitation, whereas the energy profile corresponding to the chromophore deprotonation is dramatically affected. One should take into account that the above discussion is entirely static, based on prospects of the potential energy landscape of the proton wire, which nonetheless provides much fundamental insight.

(43) Kennis, J. T. M.; Larsen, D. M. van Stokkum, I. H. M.; Vengris, M.; van Thor, J. J.; van Grondelle, R. *Proc. Natl. Acad. Sci. U.S.A.* **2004**, *101*, 17988−17993.

Dynamical studies need to be conducted in the future to clarify the operation of the GFP proton wire. This is currently work in progress in our laboratory. However, the simulations and results given in this article provide fundamental insight in the energetics and operation of the proton wire in GFP. Concretely, the results presented point in the direction of an effective competition between the best of the stepwise mechanisms and a fully concerted mechanism. The results are relevant as a complement to the experimental work devoted to understand the mechanism of photoactivated proton wires, their importance in biology, and technological applications. They also constitute a starting point of new and deeper theoretical work in this exciting field of research.

Acknowledgment. R.G. acknowledges the Ministerio de Educación y Ciencia for a Ramón y Cajal research contract. We are grateful for financial support from the Ministerio de Educación y Ciencia and the Fondo Europeo de Desarrollo Regional through Project CTQ2005-07115/BQU, and from the DURSI de la Generalitat de Catalunya (2005SGR00400).

Supporting Information Available: Complete list of authors for refs 35 and 40. A table containing the energy of the 252 structures used in the construction of the proton-transfer energy profiles at both CASSCF and CASPT2 levels with the (6,6) active space for the S_0, $^1\pi\pi^*$, and $^1\pi\sigma^*$ electronic states. Absolute energies and geometrical structures of the eight protonation states considered in the discussion. This material is available free of charge via the Internet at http://pubs.acs.org.

JA0549998